V European Conference on Computational Fluid Dynamics
ECCOMAS CFD 2010
J. C. F. Pereira and A. Sequeira (Eds)
Lisbon, Portugal,14-17 June 2010

IMPLICIT AND SEMI-IMPLICIT TREATMENTS FOR MHD COMPUTATIONS

Rony Keppens*, Allard-Jan van Marle† and Chun Xia††

*Centre for Plasma Astrophysics, K.U.Leuven
Celestijnenlaan 200B, 3001 Heverlee, Belgium
& FOM-Institute for Plasma Physics Rijnhuizen
Nieuwegein, The Netherlands
& Astronomical Institute, Utrecht University, The Netherlands
e-mail: Rony.Keppens@wis.kuleuven.be

†Centre for Plasma Astrophysics, K.U.Leuven
e-mail: AllardJan.vanMarle@wis.kuleuven.be

°Nanjing University, Nanjing, China
e-mail: 99xc41@gmail.com

Key words: Magnetohydrodynamics, numerical methods, (semi-)implicit treatments

Abstract. *We recall some general guidelines for implicit and semi-implicit time integration schemes, using early examples of (semi-)implicit MHD tests[1,2]. We point out their means to handle the Jacobian evaluation, and the solution strategy for the linear system solves, since implicit schemes typically require the solution of large linear systems containing the Jacobian matrix.*

As more recent, specific applications, we discuss parallel, grid-adaptive computations that use semi-implicit treatments for handling local source terms. They cover idealized stellar outflow models with local radiative losses, which demonstrate how grid-adaptivity as well as implicit source treatments may both be inevitable[3]. Our second application combines optically thin loss terms with thermal conduction, addressing the dynamic formation of a prominence in the solar, magnetized corona. Assuming a given magnetic loop geometry, this simulation solves for the plasma dynamics under the influence of gravity, pressure gradients, thermal conduction, optically thin radiative losses and an assumed background heating. These applications illustrate the basic building blocks required for future, even more realistic MHD simulations.

1 INTRODUCTION

Magnetohydrodynamics (MHD) governs the large-scale behaviour of the fourth state of matter, where ions and electrons collectively behave in a fluid-like, plasma state. In ideal MHD, where we deal with pure conservation laws (mass, momentum, total energy and magnetic flux) ruling the dynamics of plasmas, the existence of three distinct wave speeds and types can already pose severe challenges to the traditional explicit time stepping approaches. Such explicit methods to time-advance the discretized PDEs on a grid invariably connect the temporal advance Δt with the instantaneously smallest grid spacing Δx by the overall largest wave speed $c_{\max}$ through the Courant-Friedrichs-Lewy condition, expressing $\Delta t < \Delta x/c_{\max}$. The geometry of the magnetic configuration, which due to the divergence-free condition on the magnetic field $\mathbf{B}$ is of a flux-tubular variety, then combines to introduce potentially very disparate timescales for Alfvén versus slow/fast magnetoacoustic waves. These speeds also depend on the relative importance of the local field $\mathbf{B}$ as measured with the ratio of plasma to magnetic pressure $\beta = 2p/B^2$, and it may turn out prohibitive to face the restriction on the timestep invoked by the fast magnetoacoustic wave, when e.g. only a steady-state solution to the equations is of interest. The problem becomes even more pronounced when wanting to time-integrate the dynamics of plasmas where additionally visco-resistive effects are at play, since diffusion like terms would otherwise introduce a stability restriction of the form $\Delta t < (\Delta x)^2/d_{\max}$, with $d_{\max}$ a diffusion-related transport coefficient (such as resistivity, viscosity, thermal conduction). In all such cases, one can resort to implicit time integration strategies, which although algorithmically more involved, can become computationally advantageous as they lift the *stability* constraint on the allowed time step Δt (however, the use of larger timesteps may impact *accuracy* when time evolutions are of interest). Many variants of (semi-)implicit treatments have been demonstrated on plasma dynamical problems, and in this contribution, we briefly recall two typical, early examples of implicit strategies in an MHD context. These relate to an effort in the late nineties[1,2] to develop a versatile software tool for solving systems of (near-)conservation laws, encompassing in particular hydro and MHD modules with optional source terms. Meanwhile, this 'Versatile Advection Code' (VAC[4]) has been applied to a fair variety of astrophysical to laboratory motivated plasma studies. We also provide an update on a contemporary follow-up to this code, the MPI-AMRVAC software[5] incorporating a parallelized block-adaptive strategy for classical up to relativistic hydro and MHD systems. While this latest code deliberately restricted time stepping strategies to (grid-level dependent) shock-capturing explicit schemes, we report on recent applications where in essence hydrodynamical evolutions use semi-implicit treatments for selected source terms. The paper concludes with an outlook to future challenges where (semi-)implicit strategies will be invaluable.

2 EARLY TESTS FOR IMPLICIT MHD

The MHD equations can be written in the form

$$\partial_t \vec{U} = \vec{R}(\vec{U}) = -\sum_i \partial_i \vec{F}_i(\vec{U}) + \vec{S}(\vec{U}, \partial_i \vec{U}, \partial_i \partial_j \vec{U}, \mathbf{x}, t), \tag{1}$$

where t is the time, i and j indicate components of the spatial coordinate $\mathbf{x}$, while $\vec{U}$ denotes the vector of conservative variables (mass, momentum, total energy density and $\mathbf{B}$). The right hand side $\vec{R}$ is the residual, which for steady-state problems must be made to vanish. It contains the sources $\vec{S}$ and the divergence of fluxes joined in $\vec{F}_i$.

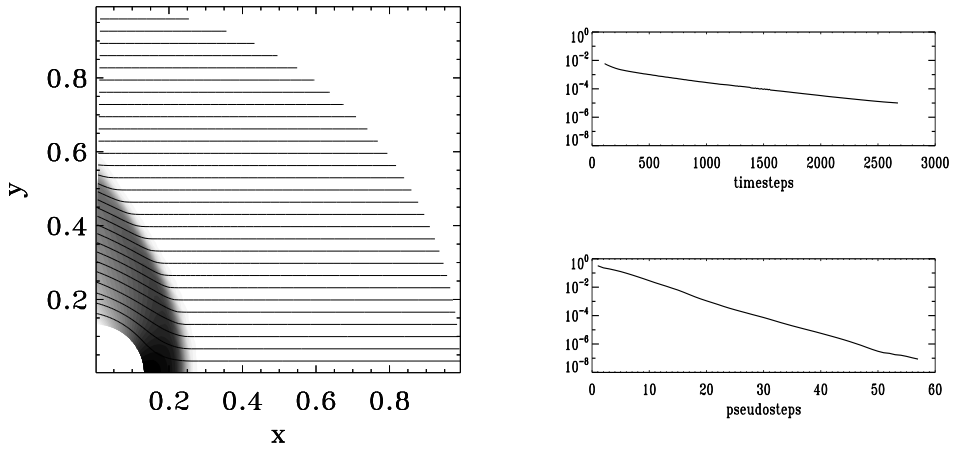

Figure 1: Steady, magnetized bow shock about a conducting cylinder, taken from Tóth et al.[1]. Left panel: field lines and a greyscale contour plot of the density. Right panels: The (normalized) residual evolution versus CFL-limited timesteps (top) and versus implicit pseudosteps (bottom).

In case one is interested in a steady-state solution, one can use a fully implicit backward Euler scheme, which after linearization amounts to solving

$$\left[\frac{\hat{I}}{\Delta t} - \frac{\partial \vec{R}_{\rm impl}}{\partial \vec{U}}\right]\left(\vec{U}^{n+1} - \vec{U}^{n}\right) = \vec{R}(\vec{U}^{n}). \tag{2}$$

Note that the Jacobian matrix $\partial \vec{R}_{\rm impl}/\partial \vec{U}$ may exploit a different discretization for $\vec{R}_{\rm impl}$ than the typically second order evaluation for the residual $\vec{R}$ (and that one may also consider semi-implicit variants which only treat some variables, or sources, implicitly). As a concrete example, we recall the computation of a magnetized bow shock flow about a perfectly conducting cylinder[1]. When we take the plasma beta of the upstream flow $\beta = 2$ and take a horizontal flow at Alfvén mach number $M_A = |v_x|\sqrt{\rho}/B = 4$, the flow settles into a steady pattern shown in Figure 1. The problem is solved on a polar grid, and the convergence history of both explicit and implicit strategies (which we refer to as

pseudo-timestepping) for obtaining the steady state are shown at right in Figure 1. The convergence is here expressed as a relative change from one (pseudo-)time level to the next, taking all conservative variables into account. In this steady problem, the implicit strategy uses a first order approximation in $\vec{R}_{\rm impl}$ which directly corresponds to a low order Total Variation Diminishing Lax-Friedrichs (TVDLF) scheme. The Jacobian is block penta-diagonal, and an incomplete LU-decomposition based preconditioner is exploited to accelerate the convergence of the iterative, bi-conjugate gradient linear system solver.

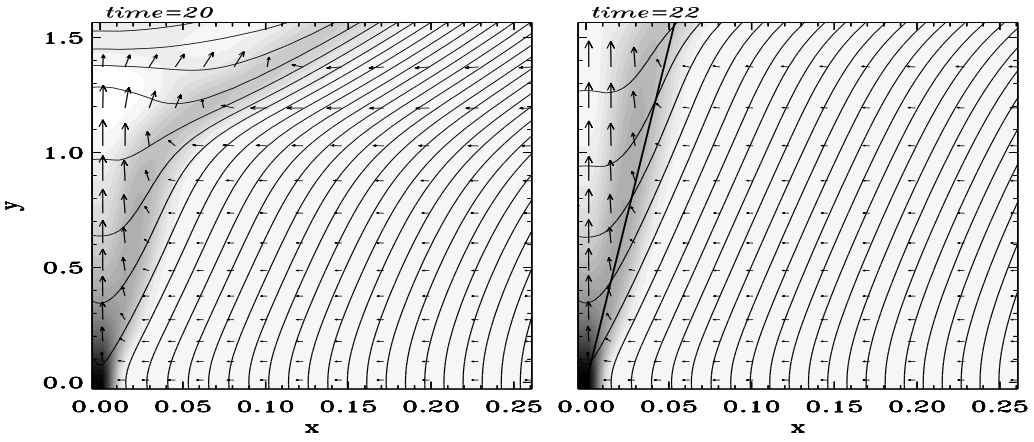

Figure 2: Evolution of a planar magnetic reconnection problem[1]. A localized resistive layer (lower left corner) controls the evolution, shown by means of field lines, velocity field arrows, and a greyscale plot of the current density.

While the previous example focused on a steady-state computation, a strategy for implicit, time-accurate computations was demonstrated on a planar resistive MHD problem as well[1]. The second order accurate, 3-level Backward Differentiation Formula writes as

$$\begin{aligned}\vec{U}^{n+1} &= \vec{U}^n + \Delta t \vec{R}(\vec{U}^n) + \frac{1}{3}\Delta t \left[\frac{\vec{U}^n - \vec{U}^{n-1}}{\Delta t} - \vec{R}(\vec{U}^n)\right] \\ &\quad + \frac{2}{3}\Delta t \left[\vec{R}_{\rm impl}(\vec{U}^{n+1}) - \vec{R}_{\rm impl}(\vec{U}^n)\right], \end{aligned} \tag{3}$$

and by restricting the Jacobian appearing when linearizing $\vec{R}_{\rm impl}(\vec{U}^{n+1})$ to the ideal MHD terms, one can again use the first order variant of the TVDLF scheme while dealing with the larger-stencil, resistive sources explicitly (hence the distinction between $\vec{R}$ and $\vec{R}_{\rm impl}$). This was done to obtain the evolution towards a shock-dominated, fast reconnection configuration shown in Figure 2. The figure shows how a small diffusion region, by symmetry located in the lower left corner of the domain, actually controls the dynamical adjustment of a current layer to a Petschek-type configuration: field lines reconnect and flux is expelled from the small diffusion region at Alfvénic velocities along the symmetry

axis. A pair of slow magnetosonic shocks forms across which the plasma is diverted and accelerated.

3 LOCAL SOURCE TERM TREATMENTS

3.1 Current code status

The VAC code from the examples of the previous section is still in use today in both laboratory and astrophysical communities: García-Martínez and Farengo[6] recently applied the code to study the relaxation of spheromak, kink-unstable MHD equilibria in 3D, visco-resistive, isothermal MHD simulations. Soenen et al.[7] demonstrated numerically in axisymmetric, ideal MHD that a series of coronal mass ejections (CMEs) can originate from an initial triple arcade structure in the solar corona, energized by shearing the arcade system at the solar surface. Both these efforts use a suitably adapted version of the community code, and employ explicit schemes throughout: the effects of resistivity in the spheromak study is important but the instability timescale is in essence found from ideal MHD, forcing an explicit treatment. The latter, CME investigation uses the common approach that reconnection events can be amenable to numerical modeling, even if only numerical resistivity (i.e. truncation level errors) can account for it.

As a modern descendant of the VAC code, the MPI-AMRVAC code[5] has meanwhile evolved to a similarly versatile software to handle systems of the form (1) in any dimensionality in a parallelized, grid-adaptive framework. The grid-adaptivity is currently of a block-adaptive kind, where in 3D, gridblocks get subdivided in 8 blocks all using as basic gridelement $(\Delta x/2)(\Delta y/2)(\Delta z/2)$. The finer meshed gridblocks can also be dynamically removed if need be, with refine and coarsen actions depending on a combination of user- and application-specific (de-)refinement criteria as well as automated error estimators, exploiting approximations to local second derivatives. The parallelization is achieved by means of a space-filling Morton (Z-order) curve to load-balance the simulation dynamically, trying to keep the number of blocks per processor optimally distributed. The actual systems of equations precoded in MPI-AMRVAC include pure advection, the Euler equations, special relativistic gas dynamics, ideal and resistive MHD, and special relativistic ideal MHD. The latest applications concentrate on relativistic astrophysical flows[8], and fully exploit the Adaptive Mesh Refinement (AMR) as well as the availability of several shock-capturing, explicit discretization schemes. In what follows, we give recent examples where the AMR approach has been combined with implicit source term treatments, in particular incorporating the effects of optically thin radiative losses, ultimately combined with thermal conduction.

3.2 Radiative losses and the need for AMR

In a fair variety of astrophysical applications, one needs to account for energy losses through radiative processes. In the simplest case, these represent local energy loss terms

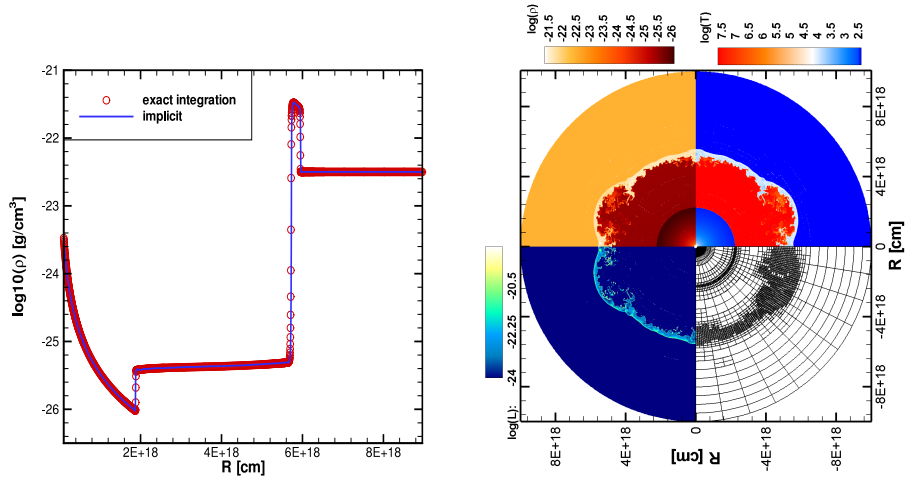

Figure 3: Stellar wind simulations with local radiative loss terms[3]. Left panel: a spherically symmetric simulation, comparing an exact with an implicit solution. Right: a 2D simulation, showing clockwise from bottom right: grid, luminosity, density and temperature.

proportionate to the density squared, in a form like

$$\frac{\partial e}{\partial t} \; + \; \nabla \cdot ((e+p)\mathbf{v}) \;\; = \;\; -\,\rho^2 \Lambda(T). \tag{4}$$

The above form is adequate for gas dynamical situations where the total energy density is derived from pressure p and density ρ through $e \; = \; \frac{1}{2}\rho v^2 \; + \; \frac{p}{(\gamma-1)}$, but a very similar (and identical source) term applies for the MHD case as well. Due to its local dependence, the term is easily handled semi-implicitly, where only the source addition happens implicitly, introducing a Newton-Raphson procedure. What is particular for such optically thin radiative losses, is the fact that the cooling function $\Lambda(T)$ is of a tabulated variety, with strong variations in certain temperature intervals, needing suitable interpolation formulae. As the cooling timescale, set by

$$\tau_{\rm cool} \;\; \sim \;\; \frac{p}{\rho^2 \Lambda(T)}, \tag{5}$$

can be much shorter than the one associated with sound wave propagation, an implicit treatment is warranted. In van Marle and Keppens[3], we recently demonstrated the need for adequate source term treatments in highly idealized stellar wind expansion studies. In a 1D spherical hydro flow we impose at the lower radial boundary a mass loss rate and speed typical for a supersonic wind of a massive star. This high speed, low density spherical outflow impacts a uniform interstellar medium (ISM), and Figure 3, left panel shows the density profile at a representative instant in time. One notes from left to right the wind profile through which density decreases with radius, the reverse shock transition to shocked wind matter, the contact discontinuity, the swept-up, shocked ISM material

occupying a thin shell of high density matter, up to the foreward shock transition to the uniform ISM. The figure compares two means for incorporating the cooling source term, an exact method against an implicit treatment, which are seen to coincide. The radiative losses in this simulation have dynamically influenced the evolution, as the shocked ISM shell is significantly narrowed due to the energy losses, and this in turn translates to a need for grid-adaptivity (4 levels where employed in Figure 3). The right panel gives an impression of a similar, two-dimensional result, where the cooled, shocked shell is distorted due to Rayleigh-Taylor instabilities that originated at the contact discontinuity.

3.3 Prominence formation

A final example of more recent work where semi-implicit, source term treatments have been used in parallel, grid-adaptive studies is from an ongoing study targeting the formation of prominence condensations in the solar atmosphere. These prominences represent material that is 100 times denser and cooler than the surrounding plasma in the solar corona, which in turn is heated to million degrees Kelvin. They consistently form in 'dipped' magnetic configurations, i.e. in upwardly curved magnetic loops, such that the upward Lorentz force can balance the pull of gravity on this dense material. Observations show that they appear to lie above magnetic neutral lines seperating magnetic field regions of opposite polarity, and that the magnetic field is primarily aligned with the prominence axis. These observational facts, along with the dynamical dominance of the magnetic field in the solar corona (low β) justifies the use of a 1D model where the field configuration is given, i.e. the magnetic loop is then in essence a rigid pipe along which we solve for the plasma dynamics. The study then merely focuses on the prevailing thermodynamic conditions along a loop from photospheric regions all the way through the corona, and aims to identify the thermal instability process as the ultimate cause for prominence formation.

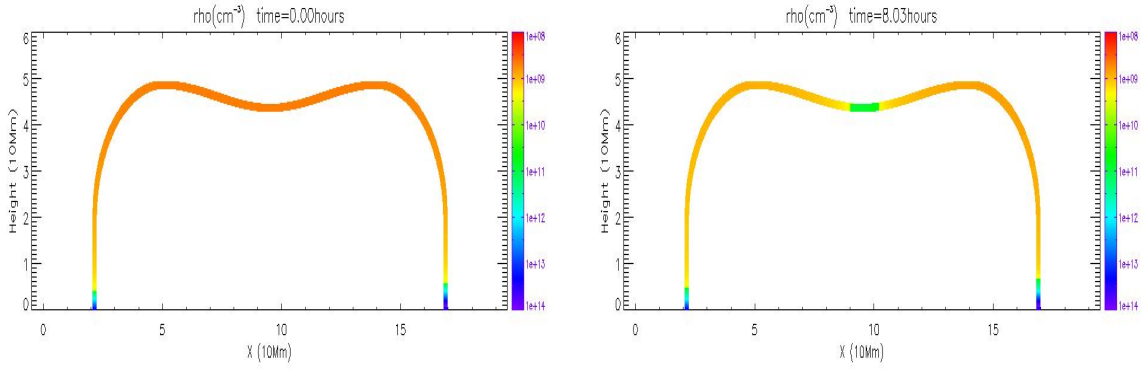

Figure 4: Prominence formation along a dipped magnetic loop. The assumed magnetic loop shape is shown, with the density distribution in a colorscale along the loop. A prominence has formed by thermal instability in the dipped region, and has already grown to a relatively large size in the right panel.

The 1D equations consider mass conservation, Newton's law where pressure gradients

as well as loop-projected gravity is taken along, and the energy equation considered then takes the form

$$\frac{\partial e}{\partial t} + \frac{\partial}{\partial s}\left((e+p)v\right) = \rho v g_{\parallel} + \frac{\partial}{\partial s}\left(\kappa T^{5/2}\frac{\partial T}{\partial s}\right) + \rho h(s,t) - \rho^2\Lambda(T). \tag{6}$$

Note how we now solve for density $\rho(s,t)$, total energy density $e(s,t)$ and velocity $v(s,t)$ along the loop with fieldline projected gravity $g_{\parallel}$ and the inclusion of thermal conduction with conduction coefficient κ. A prescribed (spatio-temporal) background heating function enters through $\rho h(s,t)$, which we fix in a variety of ways. The initial condition for our study of prominence formation then first relaxes an initial hydrostatic atmosphere with prescribed temperature variation to the one expressing full thermodynamic balance along the loop. The inclusion of thermal conduction and heating causes this relaxed endstate to closely follow the observed dramatic changeover in temperature when going from photosphere/chromosphere to solar coronal regions, with a markedly sharp rise in temperature at the transition region (from a few 1000 Kelvin to million degrees). From this relaxed state, we then vary the heating $h(s,t)$ and follow the formation of a thermal condensation once the isobaric criterion, given by

$$\left.\frac{\partial}{\partial T}\left(\rho\Lambda(T) - h\right)\right|_p < 0, \tag{7}$$

gets violated locally. The AMR is vital to capture the rapid, extremely local nature of this thermal instability accurately. Again, the condensation process is ultimately connected to the detailed tabulated variation of optically thin radiative losses in $\Lambda(T)$. The simulation uses the same implicit approach for the local loss term as in the previous example, and also treats the thermal conduction term implicitly. This latter source is discretely handled by solving a tridiagonal system for the new temperature values T_i^{n+1} where i denotes the grid point index. This system writes for the update in internal energy the discrete approximation

$$\frac{\partial[\rho T/(\gamma-1)]}{\partial t} = \frac{\partial}{\partial s}\left(\kappa T^{5/2}\frac{\partial T}{\partial s}\right) \Rightarrow a T_{i-1}^{n+1} + (c-a-b)T_i^{n+1} + b T_{i+1}^{n+1} = c T_i^n$$

$$\text{where} \quad a \equiv -\kappa\frac{\left(\sqrt{T_{i-1}^n T_i^n}\right)^{2.5}}{(\Delta s)^2}, b \equiv -\kappa\frac{\left(\sqrt{T_{i+1}^n T_i^n}\right)^{2.5}}{(\Delta s)^2},$$

$$\text{while} \quad c \equiv \frac{\rho_i^n}{(\gamma-1)\Delta t}\,.$$

On each block of the AMR hierarchy, we loosely couple the grid blocks using previous time level ghost cell values, or by fixing the previous gradient there. On selected tests, this was found to adequately handle the otherwise stiff source term.

4 CONCLUSIONS AND OUTLOOK

In future applications, we target multi-dimensional MHD problems where the availability of automated grid-adaptation and implicit source term treatments is necessary. A concrete example is the extension of the prominence formation modeling to its realistic, 3D manifestation. This kind of modeling will require highly scalable parallel code, where all aspects illustrated above return: we will need to first evolve the 3D background structure to a steady configuration, in which radiative losses, thermal conduction and heating terms play key roles. This evolution towards steady state is likely to involve reconnection processes, suggested by observations. To follow the spontaneous formation of a prominence by thermal instability, high effective resolution through AMR will be warranted. The implicit treatment of thermal conduction in multi-D, block adaptive simulations will thereby be an essential ingredient.

Acknowledgments. We acknowledge financial support from FWO, grant G.0277.08 and from the K.U.Leuven GOA/09/009. Part of the computations made use of the High Performance Computing VIC cluster at K.U.Leuven.

REFERENCES

[1] G. Tóth, R. Keppens and M.A. Botchev, Implicit and semi-implicit schemes in the Versatile Advection Code: numerical tests, *Astron. & Astrophys.*, **332**, 1159 (1998)

[2] R. Keppens, G. Tóth, M.A. Botchev and A. van der Ploeg, Implicit and semi-implicit schemes: algorithms, *Int. J. Numer. Meth. Fluids*, **30**, 335 (1999)

[3] A.J. van Marle and R. Keppens, Radiative cooling in numerical astrophysics: the need for adaptive mesh refinement, *Comp. in Fluids*, submitted (2010)

[4] G. Tóth, A general code for modeling MHD flows on parallel computers: versatile advection code', *Astrophys. Lett. Commun.*, **34**, 245 (1996)

[5] B. van der Holst and R. Keppens, Hybrid block-AMR in cartesian and curvilinear coordinates: MHD applications, *JCP*, **226**, 925 (2007)

[6] P.L. García-Martínez and R. Farengo, Relaxation of spheromak configurations with open flux, *Phys. of Plasmas*, **16**, 112508 (2009)

[7] A. Soenen, F.P. Zuccarello, C. Jacobs, S. Poedts, R. Keppens and B. van der Holst, Numerical simulations of homologous coronal mass ejections in the solar wind, *Astron. & Astrophys.*, **501**, 1123 (2009)

[8] Z. Meliani and R. Keppens, Decelerating relativistic two-component jets, *Astrophys. J.*, **705**, 1594 (2009)